Analysis of the vane test considering size and time effects

by A. Pérez–Foguet, A. Ledesma and A. Huerta

Escuela Técnica Superior de Ingenieros de Caminos
Universitat Politècnica de Catalunya (UPC)

c/ Jordi Girona 1-3, 08034 Barcelona, Spain

Corresponding author e–mail: huerta@etseccpb.upc.es

Publication CIMNE No. 122
First Draft, October, 1997

Submitted to *Int. J. for Numerical and Analytical Methods in Geomechanics*
Second Draft, November, 1997

Accepted for publication in *Int. J. for Numerical and Analytical Methods in Geomechanics*
April, 1998

SUMMARY

An analysis of the vane test using an Arbitrary Lagrangian – Eulerian formulation within a finite element framework is presented. This is suitable for soft clays for which the test is commonly used to measure 'in situ' undrained shear strength. Constitutive laws are expressed in terms of shear stress – shear strain rates, and that permits the study of time effects in a natural manner. An analysis of the shear stress distributions on the failure surface according to the material model is presented. The effect of the constitutive law on the shear band amplitude and on the position of the failure surface is shown. In general, the failure surface is found at 1. to 1.01 times the vane radius, which is consistent with some experimental results. The problem depends on two dimensionless parameters that represent inertial and viscous forces. For usual vane tests, viscous forces are predominant, and the measured shear strength depends mainly on the angular velocity applied. That can explain some of the comparisons reported when using different vane sizes. Finally, the range of the shear strain rate applied to the soil is shown to be fundamental when comparing experimental results from vane, triaxial and viscosimeter tests. Appart from that, an experimental relation between undrained shear strength and vane angular velocity has been reproduced by this simulation.

1. INTRODUCTION

The vane shear test has been used extensively from the 50's to measure the 'in situ' shear strength of soft clays, due to the simplicity of the test and to the difficulties in obtaining undisturbed samples in these materials. In fact most site investigation manuals and codes of practice in geotechnical engineering include a description of the vane equipment and some recommendations for its use.[1,2] Also, the vane test has been useful in characterizing the 'in situ' behaviour of very soft materials like slurried mineral wastes and in the determination of the viscosity of plastic fluids in laboratory tests.[3,4] However, in spite of its common use, the interpretation of the vane test has been quite often a controversial issue. The work presented by Donald et al.[5] summarizes the main drawbacks of the test and the usual sources of error in the estimation of the undrained strength: soil anisotropy effects, strain rate effects, and progressive failure. Classical interpretation of vane results did not take into account those effects. To overcome these difficulties, some research has been devoted to the experimental analysis of the vane test in the laboratory or in the field: Menzies and Merrifield[6] measured shear stresses in the vane blades, and Matsui and Abe[7] measured normal stresses and pore pressures in the failure surface. Also Kimura and Saitoh[8] obtained pore water pressure distributions from transducers located in the vane blades.

On the other hand, numerical simulations of the vane test are scarce, due to its mathematical complexity. Donald et al.[5] presented a three-dimensional (3D) finite element analysis of the vane using a linear elastic constitutive model. Matsui and Abe[7] also compared their experimental results with a coupled 2D finite element simulation using a strain-hardening model. More recently, De Alencar et al.[9] and Griffiths and Lane[10] have presented 2D finite element simulations of the vane with a strain-softening constitutive law. The latter also showed stress

distributions in a quasi 3D analysis. These experimental and numerical reports have improved the knowledge of the stress distributions around the failure surface and therefore have contributed to an improvement on the interpretation of the vane test. Nevertheless, there is still some concern about the validity of the undrained strength $(s_u)_{vane}$ obtained in this way. Bjerrum[11] proposed a correction factor for the vane undrained strength which decreased with plasticity index. Also Bjerrum proposed to extend the procedure considering two correction factors in order to take into account anisotropy and time effects. That correction has been improved using information from case histories of embankment failures.[12] Despite this correction factor, important differences between corrected $(s_u)_{vane}$ and undrained shear strength measured with independent tests have been reported for some clays.[13,14,15] The contradictory results presented by different authors show that conceptual analyses of the vane test are still required to establish the validity of the test. As there are several factors influencing the result, it is difficult to deal with all of them simultaneously. Even some probabilistic approaches have been presented elsewhere to deal with the uncertainties involving the 'in situ' measurement of the mobilized undrained shear strength.[16] Recently, a new model to estimate a theoretical torque based on critical state concepts have been presented.[17,18] Comparing theoretical and measured torques from a literature survey, they have defined a correction factor similar to that proposed by Bjerrum, although more elaborated.

In this paper, a particular approach to the vane test that allows one to study size and time effects in a natural way is presented. Also some results concerning the failure mechanism are presented and compared with the ones obtained from classical solid mechanics simulations. One of the difficulties associated to the numerical analysis of the vane test is dealing with large deformations and the strain localized zone produced in the failure area. Even some of the large - strain finite element models have disadvantages when large local deformations are involved. The problems derived from the distortion of elements can be avoided if an Arbitrary Lagrangian – Eulerian formulation (ALE) coupled to the Finite Element Method is used. In a Lagrangian formulation mesh points coincide with material particles. Each element contains always the same amount of material and no convective effects are generated. In this case the resulting expressions are simple, but it is difficult to deal with large deformations. On the other hand, a Eulerian formulation considers the mesh as fixed and the particles just move through it. Now convective effects appear due to the relative movement between the grid and the particles, but it is possible to simulate large distortions. An ALE formulation reduces the drawbacks of the purely Lagrangian or Eulerian formulations, and it is appropiate when large deformations are expected. For this reason the method was first proposed for fluid problems with moving boundaries[19,20] and has been used in this paper to analyze the vane test. Following that approach, the material involved in the vane test has been simulated as a plastic incompressible fluid. That would take into account the large strains involved in the test. Also, the rate of rotation may be easily considered as velocities instead of displacements are the main variables. The fact that the vane test is more appropiate for very soft materials makes reasonable the analysis using a constitutive law for a plastic fluid. Applications of ALE to Geomechanics using classical elastoplastic constitutive laws for solids have been published elsewhere.[21,22,23]

In next section, the main characteristics of vane test are outlined, pointing

out some of the drawbacks of the test that complicate its interpretation. Then a basic description of the theoretical constitutive laws used in this paper is presented. Also the equations involved in the problem, taking into account the ALE formulation, are shown. A dimensionless formulation allows the definition of some combination of parameters that control the mathematical problem. These dimensionless numbers can explain the variability of vane results reported in some previous works. Then some applications to theoretical fluids and to real materials (soft clay and slurry red mud) are presented. These examples show a close dependency between amplitude of the strain localized zone, type of failure during the test, and constitutive models considered and are useful to clarify the interpretation of the vane test.

2. MAIN FEATURES OF FIELD VANE TEST

There is a general agreement concerning the essential geometry of the vane. Figure 1 shows the main elements of the equipment and its usual dimensions.[24] Although there are other configurations with different shapes and number of blades,[26] the most popular one consists of four rectangular blades with a ratio H/D of 2:1. The test is performed by rotating the central rod (usually by hand) and measuring the torque applied. This produces a cylindrical shear surface on the soil, and therefore the maximum torque measured is related to the undrained shear strength of the material, s_u. Despite its simple use, the interpretation of the test is not always straightforward. A few shortcomings of the test have been reported during the last thirty years, mainly related to the stress distributions on the failure surfaces and to the influence of time on the results.

Stress distributions

The distribution of stresses around the failure surface is not always uniform, although the usual expressions presented in the codes of practice to compute s_u from the torque assume that uniformity. Two causes have been reported as main origin of non-uniformity: soil anisotropy and progressive failure.

The total torque, T, is employed in creating a vertical cylindrical failure surface and, also, two horizontal failure surfaces in the top and the bottom of the material involved in the test. Thus $T = T_v + T_h$, where each term corresponds to the contribution of the torque from each failure surface. If the stress distribution is assumed constant in all surfaces then, by limit equilibrium, it is possible to evaluate

$$T_v = \frac{1}{2}\pi D^2 H s_u \qquad \text{and} \qquad T_h = \frac{1}{6}\pi D^3 s_u \tag{1}$$

where D and H are the diameter and the height of the vane respectively. If the maximum torque during the test, T, is measured, then, from (1)

$$s_u = \frac{T}{\pi\left[\left(\frac{D^2 H}{2}\right) + \left(\frac{D^3}{6}\right)\right]}, \tag{2}$$

or for a vane of height equal to twice its diameter

$$s_u = \frac{T}{3.66 D^3} \qquad \text{and} \qquad \frac{T_h}{T_v} = \frac{1}{6}. \tag{3}$$

The stress distributions obtained from experiments or from numerical analyses are partly different from the assumptions above considered. For instance, figure 2 shows the stress distributions on the failure surfaces measured in the blades of an instrumented vane,[6] and it may be seen that the distribution of shear stresses on the top is very different from the uniform assumption. Numerical results using an elastic constitutive law[5] already suggested a nonlinear distribution of stresses in the top of the vane (figure 3a). From these results Wroth[27] proposed a polynomial function to represent the shear stress distribution $\tau = \tau(r)$ at the top and bottom surfaces, and therefore

$$\tau = s_u \left(\frac{r}{D/2} \right)^n \qquad \text{and} \qquad T_h = \frac{\pi D^3 s_u}{2(n+3)} \tag{4}$$

where r is indicated in figure 3a. Wroth suggested a value of $n = 5$ for London clay, based on the results from Menzies and Merrifield.[6] For this value, the torque ratio becomes smaller: $T_h/T_v = 1/16$. Hence, the contribution of the horizontal failure surfaces to the total torque seems to be less significant in practice. That is, almost 94% of the resistance to torque is provided by the vertical failure surface. As a consequence of that, classical expressions to obtain s_u would underestimate the actual value of shear strength and that has been reported by some authors.[27,28]

Equation (4) is quite general as according to the value of n different stress distributions for the top and bottom of the vane can be considered. From that results it seems that a value about $n = 5$ could be appropiate. However, some authors have confirmed recently values close to $n = 0$ for different soils,[26] which corresponds again to a uniform stress distribution. A finite element analysis presented by Griffiths and Lane[10] confirms that for elastoplastic materials the shear stress can be close to a constant value on the top of the vane (figure 3b). They also showed an elastic analysis which is consistent with that presented by Donald et al.[5] Therefore, the value of n will depend on the stress state reached on the top and bottom of the vane, and that is difficult to predict in advance. This conclusion assumes that soil is isotropic, which is not always the case. When the soil is anisotropic, the interpretation of the test becomes more difficult, as, for instance, maximum shear stress can be reached in the vertical surface whereas the situation on the top is still elastic. As the result used from the test is the peak of the curve torque - rotated angle, which is in fact an integral of all these stresses, it is difficult to distinguish all these effects from just one measured value. As the vane includes vertical and horizontal failure surfaces, some attempts have been made to identify anisotropy by means of vanes with different dimensions and shapes in order to estimate T_h and T_v separately.[29,30,5] Bjerrum[11] proposed a correction factor to account for the anisotropy that has been critiziced in some cases.[31,15]

When the soil is isotropic and is not strain softening, as the maximum shear strains are produced at $r = R_v$, where R_v is the vane radius, it is expected to reach the maximum shear stress at the vertical surface failure. If this value is kept constant, then plastification of the top and bottom vane will occur and the peak measured torque will correspond to a uniform distribution of shear stresses in all surfaces. However, if the soil has a strain softening constitutive law, the shear stress on the vertical failure will decrease and the peak torque will correspond to an intermediate situation and $n > 0$. Moreover, when strain softening

occurs, the shear stress is not constant, which makes the result of the vane test insufficient to estimate s_u. These arguments are consistent with the conclusions obtained by De Alencar et al.[9] in a 2D numerical analysis. They simulated the vane using different strain softening constitutive laws (but all of them with the same peak shear strength). The torque - rotation curve was totally dependent on the constitutive law employed. Numerical simulations presented by Griffiths and Lane[10] (figure 3b) present the same dependence. All those results showed the influence of progressive failure on the final interpretation of the test.

A consequence of all the works involved in the study of the interpretation of the vane is that the complete stress - strain curve of the material and its anisotropy must be known in advance in order to explain correctly the results of the test. However, for isotropic soft materials it seems to be an appropiate test, and the vertical failure surface would be predominant in that case.

Time effects

The influence of time on the results of the test has two different aspects: the delay between insertion and rotation of vane, and the rate of vane rotation. The disturbance originated by the vane insertion and the consolidation following that insertion are difficult to predict in general. There are a few experimental studies about these effects. They suggest that in order to reduce the vane insertion effects, blade thickness related to vane size must be as small as possible.[32,33] On the other hand, the delay on carrying out the test after vane insertion increases the measured shear strength, due to the dissipation of pore water pressures originated by the insertion and also due to thixotropic effects. This effect is usually not considered in vane analyses, but there is experimental evidence on the high pore pressure developed by vane insertion[8] and on the microestructural changes due to thixotropic phenomena.[34] Results from Torstensson[33] show that within five minutes after insertion measured shear strength does not change. It must be pointed out that both effects depend on the type of clay involved in the test (sensitivity, consolidation coefficient c_v, etc.). Fabric disturbance due to insertion reduces the true undrained strength in about 10%, but if consolidation after insertion is permitted a 20% increase on strength is produced.[24] The standard vane test is usually performed 1 minute after the insertion of the blades, which is the maximum delay value suggested by Roy and Leblanc.[25] In that case, no consolidation is allowed.

The effect of the rate of vane rotation on the interpretation of the test is also important. The standard rate is $6 - 12^\circ$/minute. That produces failure in about 30 - 60 seconds, a shorter time than in classical triaxial tests or shear tests. Due to this difference, undrained strengths from vane tests are overestimated if compared with that obtained from classical laboratory tests. This effect can be compensated with the underestimation of s_u provided by other effects (fabric disturbance, stress uniformity,...), but their magnitude is difficult to estimate. As the vane is an undrained test, some recommendations regarding a minimum angular velocity are defined in the codes of practice. Assuming a time to failure of one minute, undrained conditions can be assured if the consolidation coefficient of the material is : $c_v \leq 3.5 \cdot 10^{-2} cm^2/s$,[24] which is usually the case when soft clays are tested. However, as in other undrained tests, measured strength increases with the velocity of the load application and this effect leads to difficulties in the interpretation of results. To consider that, Bjerrum[11]

proposed a reduction of the shear strength measured with the vane according to the plasticity index of the clay, as the usual values of shear strength obtained in the laboratory correspond to slower experiments than field vane. Measurements of vane shear strength for different velocities of rotation have been published by Wiesel[30] and Torstensson.[33] Both presented a potential expression between shear strength, s_u, and angular velocity, ω, (or time to failure) from interpolation of their results

$$(s_u)_{vane} = k_1 \omega^{k_2} \tag{5}$$

where k_1 and k_2 are constants. The value of k_2 ranged from 0.02 to 0.07. Figure 4 presents shear strength versus rotation angle for different durations of the test.[33]

The comparison of results from vanes of different shapes and different strain rates has been difficult as these effects are only related to the shear strength on the basis of empirical relations which may depend on the soil considered. A reference shear velocity: $v = \omega R_v$ as a variable to compare results from different vanes was proposed by Perlow and Richards.[35] They obtained an almost linear relationship between vane shear strength and shear velocity v for two marine sediments, but they did not have enough experimental data to propose a definite relationship. In fact some results reported by other authors,[15] show no influence of the vane radius on the measured shear strength. These differences may be due to side effects as sampling disturbance or stress relief for soils used in laboratory vane tests, which would reduce the apparent shear strength.[16] However, in general, that is taken into account when estimating s_u. This is still a controversial issue, and it will be considered later using the formulation presented in following sections.

The shortcomings presented have been extensively studied by many authors, but still there are contradictions on results and on interpretations of vane measurements. This is due to the fact that vane test is a model test rather than an element test.[17] Apart from that, other effects on vane strength have been rarely studied: for instance, influence of the stress state and K_0 (coefficient of lateral earth pressure at rest) on the result.[36,31] As a consequence of the drawbacks above mentioned, the vane test seems indicated for very soft isotropic materials. Also the dominant failure surface is the vertical one. Therefore, it is reasonable to perform numerical simulations by means of two-dimensional analyses, in order to study rate effects and stress distributions. Hence the use of plastic fluid constitutive laws and fluid mechanics equations may be appropiate to analyze time effects and to deal with this soft isotropic materials. The disturbance due to vane insertion and the 3D effects of the test are not considered within this approach.

3. CONSTITUTIVE LAWS

Soft materials have been successfully modelled by means of fluid constitutive laws to simulate classical geomechanics problems like landslides or debris flows.[37,38,39] The model is defined in terms of a shear stress – shear strain rate relationship, instead of a stress – strain one. The study of strain rate effects on soil behaviour has been considered in many works.[40,41,42,43,44] Some of them have proposed constitutive laws relating stresses with strains and strain rates to

account for time influence, based on a visco – elasto – plastic theory. Bjerrum[11] indicates that time effects in soft clays are associated with the cohesive component of the shear strength which is of a viscous nature; the frictional component of the shear strength would be further mobilized. Therefore it is not absurd to study the vane test assuming that the material involved is a plastic fluid, particularly at the beginning of the test, when viscous effects are definite. These effects depend on the type of clay considered, and plasticity index has been used historically to distinguish between different behaviours of normally consolidated clays. However, Tavenas and Leroueil[45] propose to use the limit liquid instead, because it requires only a single test and in fact the resulting correlations are essentially the same.

Let us assume that the clay involved in the test is saturated and normally consolidated. When viscous effects are studied in detail, it is found that for a particular soil (that is for a particular liquid limit w_l), the soil behaviour depends on the water content w, as shown in figure 5, from Komamura and Huang.[41] According to them, when $w > w_l$ the behaviour is viscous, that is, close to a newtonian fluid; whereas when $w < w_{vp}$ the behaviour is visco – elasto – plastic. The value w_{vp} was defined as viscoplastic limit, between plastic and liquid limits.

Results obtained in a torsional hollow cylinder are reproduced in figure 6, from Cheng.[42] The material was a Mississippi Buckshot clay with a water content close to its plastic limit. It may be seen that its behaviour is consistent with the trends established by Komamura and Huang.[41] However, further works have shown that some clays may have a visco – elasto – plastic behaviour with water content above their liquid limit.[46,47,48] Curves obtained by Locat and Demers[48] using a viscosimeter device are presented in figure 7. Note, nevertheless, that the shear rate range is different for the results reproduced in figure 6 and for those indicated in figure 7. Some consequences of this difference will be treated later. The works indicated show that fluid constitutive laws for modelling the soil behaviour have been successfully employed to account for the time effects which are supposed to be important when water content is high, but it is difficult to establish a particular behaviour for each soil state in advance.

The general constitutive equation to be used in this work is a general relationship between stresses and strain rates:

$$\sigma_{ij} = f(d_{ij}) \tag{6}$$

where σ_{ij} is Cauchy's stress tensor and the strain rate tensor is defined as

$$d_{ij} = \frac{1}{2}\left(\frac{\partial v_i}{\partial x_j} + \frac{\partial v_j}{\partial x_i}\right) \tag{7}$$

where x_i and v_i are position and velocity vectors respectively. A common expression for equation (6) is:

$$\sigma_{ij} = -p\delta_{ij} + 2\mu d_{ij} \tag{8}$$

where p is the hydrostatic pressure (tension positive) and μ is the dynamic viscosity. Equation (8) can be rewritten as

$$\sigma^d_{ij} = 2\mu d_{ij} \tag{9}$$

where σ_{ij}^d is the deviatoric stress tensor. When viscosity is assumed constant, the fluid is called newtonian. A generalized newtonian fluid is defined by a viscosity which depends on the strain rate tensor. Also, some plastic fluids show a "yield stress", that is, below that value no flow is observed, which is equivalent to an infinite viscosity in terms of equation (9). However, some authors[49] indicate that the yield stress does not exist, provided that accurate measurements are performed. That is, "yield stress" is just an idealization of the actual behaviour.

Table 1 shows a list of constitutive laws available for fluids.[20] From that list, the models by Bingham, Casson and Herschel and Bulkley seem to be most appropiate for soft materials. Those models simulate a "yield stress" value up to which no velocities or displacements occur. According to the yield stress magnitude, it is possible to reproduce effects observed in the actual behaviour of soft materials. For instance, the amplitude of the strain localized zone, the influence of the progressive failure or the brittleness of the material are supposed to be determined by the constitutive law used and specially by the existence of the "yield stress". The fluid models indicated above are consistent with experimental results like the ones depicted in figures 6 and 7, and they will be used as constitutive laws in this simulation. However, any relation between stresses and strain rates could be implemented in the formulation.

4. BASIC EQUATIONS AND ALE FORMULATION

Basic equations

Fluid movement is described by two basic equations: mass conservation equation and equilibrium equation. These equations are, respectively:

$$\frac{\partial \rho}{\partial t} + \rho \frac{\partial v_i}{\partial x_i} = 0 \qquad \text{in} \quad \Omega, \tag{14a}$$

$$\rho \frac{\partial v_i}{\partial t} + \rho c_j \frac{\partial v_i}{\partial x_j} = \rho b_i + \frac{\partial \sigma_{ji}}{\partial x_j} \qquad \text{in} \quad \Omega, \tag{14b}$$

where ρ is the density of the material, t is time, $c_j = \hat{v}_j - v_j$ where $\hat{v}_j$ is the velocity of the reference system, b_i is the mass forces vector and Ω is the domain of study. Also, repeated index means summation.

As incompressible flow is assumed, density is constant and expression (14a) leads to $\mathrm{div} v = 0$ which is equivalent to the undrained condition assumed in the standard field vane test. Introducing this result and the constitutive law presented above in (14b) gives

$$\rho \frac{\partial v_i}{\partial t} + \rho c_j \frac{\partial v_i}{\partial x_j} = \rho b_i - \frac{\partial p}{\partial x_i} + \frac{\partial}{\partial x_j}\left(\mu[\dot{\gamma}]\left(\frac{\partial v_i}{\partial x_j} + \frac{\partial v_j}{\partial x_i}\right)\right) \qquad \text{in } \Omega \tag{15}$$

where $\mu[\dot{\gamma}]$ is the dynamic viscosity, function of the shear strain rate, $\dot{\gamma} = \sqrt{2 d_{ij} d_{ij}}$.

The boundary conditions applied are $v_x = v_y = 0$ at the outer boundary and $v_x = \omega r \sin(\theta_\circ + \omega t)$ and $v_y = -\omega r \cos(\theta_\circ + \omega t)$ at the blade contours, with ω the angular velocity of the vane and $(r, \theta_\circ)$ the polar coordinates of the blade

nodes at $t = 0$. The initial stresses and velocities are considered zero in all the points and in the boundaries.

In order to find out the parameters that govern the problem, a set of dimensionless variables

$$\bar{x} = x/R^*, \qquad \bar{p} = p/\tau^*, \qquad \bar{v} = v/R^*\omega^* \quad \text{and} \quad \bar{t} = t\omega^* \tag{16}$$

is substituted in equation (15), where R^*, τ^*, ω^* are characteristic length, stress and angular velocity of the test respectively. Usually, the vane radius, R_v, is adopted for R^*, the angular velocity of the test for ω^*, and the material yield stress for τ^*. Then equation (15) is transformed into a dimensionless expression:

$$\frac{1}{Ne}\left(\frac{\partial \bar{v}_i}{\partial \bar{t}} + \bar{c}_j \frac{\partial \bar{v}_i}{\partial \bar{x}_j}\right) = -\frac{\partial \bar{p}}{\partial \bar{x}_i} + \frac{\partial}{\partial \bar{x}_j}\left(\frac{1}{NeRe}[\dot{\gamma}]\left(\frac{\partial \bar{v}_i}{\partial \bar{x}_j} + \frac{\partial \bar{v}_j}{\partial \bar{x}_i}\right)\right) \quad \text{in } \Omega \tag{17}$$

with Re and Ne equal to Reynolds and Newton number. The Reynolds number is related to viscous forces and the Newton one to inertial forces. They are defined as

$$Ne = \frac{\tau^*}{\rho(R^*\omega^*)^2} \qquad \text{and} \qquad Re = \frac{\rho\omega^*(R^*)^2}{\mu}. \tag{18}$$

The influence of Re and Ne in equation (17) is in the form of

$$N_1 = \frac{1}{Ne} = \rho\,\frac{(R^*\omega^*)^2}{\tau^*} \quad \text{and} \quad N_2[\dot{\gamma}] = \frac{1}{NeRe}[\dot{\gamma}] = \mu[\dot{\gamma}]\,\frac{\omega^*}{\tau^*}, \tag{19}$$

and their characteristic values for some typical vane tests are shown in table 2. As N_1 is much less than N_2 and accelerations usually are not large enough to compensate this difference, the inertial terms can be neglected and the problem becomes quasi-static. In these cases the problem depends just on N_2, and therefore the test will be independent of the vane radius or the fluid density. The use of those dimensionless numbers may be useful when comparing different vanes, and they will be considered later to account for size and time effects.

Computational aspects

The finite element mesh employed in the analyses is shown in figure 8. The mesh has 1492 elements and 1576 nodes, it is composed of 4 node-elements and increases the density of elements in the expected failure zone. Note that elements inside the vane failure circle have basically a rigid solid movement so a coarse mesh can be adopted there. Plane strain conditions were adopted in the simulations.

An Arbitrary Lagrangian – Eulerian (ALE) description was used for the resolution of the problem. ALE formulation has been employed to avoid the disadvantages of pure Eulerian or pure Lagrangian descriptions. If an Eulerian description is used, the mesh is fixed. That is easy to formulate, but makes difficult imposing the boundary conditions at the vane blades. On the other hand if a Lagrangian description is adopted, the nodes will follow the particle movements and mesh distortions will arise. ALE formulation can be interpreted as a combination of both descriptions: the mesh is rotated at the same velocity as the vane blades, so the soil particles have an Eulerian description; whereas

the boundary is defined in Lagrangian terms, as the mesh follows the boundaries during the test. Therefore the velocities of any node of the mesh are

$$\hat{v}_x = \omega r \sin(\theta_\circ + \omega t) \qquad \text{and} \qquad \hat{v}_y = -\omega r \cos(\theta_\circ + \omega t), \tag{20}$$

where the symbol $\hat{}$ stands for mesh prescriptions. Mesh displacements are found by integrating mesh velocities.

As a predictor – corrector algorithm is used in the numerical formulation, unknowns for time t are computed from values at time $t-\Delta t$ simulating the transient problem. Similarly to any transient problem starting from rest, boundary conditions (in this case the angular velocity of the blade) can not be discontinuous, i.e. a finite jump from zero to an imposed angular velocity which would induce an unphysical infinite angular acceleration. Therefore, a smooth variation of the angular velocity has been used. Thus, angular acceleration is always finite and becomes zero after a few time increments. As the problem is quasi-static, the acceleration is not important for the final torque, which depends mainly on the steady state value of the angular velocity reached.

As the simulation is performed by applying an angular velocity, the torque must be computed as a result of the analysis. One possibility is to estimate the torque from pressures acting on the vane blades, but in a mixed pressure – velocity formulation, the accuracy for the pressure is one order lower than the velocity. Thus, it is preferable to use an approach based on the evaluation of the power input; as the Finite Element Method is an energy based formulation. The power input, P_{input}, is the sum of two domain integrals; the first is the material time derivative of the kinetic energy of the system, while the second takes into account the variation of the internal energy:

$$P_{input} = \frac{d}{dt}\int_\Omega \frac{1}{2}\rho v_i v_i d\Omega + \int_\Omega \sigma_{ij} d_{ij} d\Omega \ . \tag{21}$$

The first term can be neglected because the vane test is quasi-static and the second one is obtained by summation of the element contributions:

$$P_{input} = T\omega \approx \sum_{i=1}^{numel} \tau_i \dot{\gamma}_i S_i \tag{22}$$

where *numel* is the number of elements and S_i the corresponding area for each element of the mesh. Note that in (22) only shear strain rates are used, as the problem has been considered incompressible. Finally, the torque applied, T, is directly obtained from that expression.

5. ANALYSES USING THEORETICAL CONSTITUTIVE LAWS

Simulations using dimensionless Bingham and Carreau models are presented in order to analyze the influence of "yield stress" in strain rate distribution. The four dimensionless constitutive laws depicted in figure 9 have been considered. These models are similar within the range considered. However, there are two main differences between them: models–1 have mainly a horizontal relation between shear stress and shear strain rate and models–2 do not, and Bingham models have a well defined "yield stress", whereas Carreau models do not. The

distribution of shear strain rates and shear stresses obtained in the simulations are represented in figure 10 (Bingham–1, Bingham–2 and Carreau–2). The shear strain rate and the particle velocity distribution over a line at 45° between blades, are depicted in figure 11. The torque actually applied while performing the test is presented, in dimensionless form, in figure 12. Also, table 3 presents some numerical values corresponding to these examples.

Note that models–1 give almost the same results, and so do models–2. The main difference between both is the more definite failure surface produced by models–1. Indeed, figure 10a shows a well defined failure surface and close to a circle of unit radius, which corresponds to the vane radius in dimensionless form. Also the amplitude of the shear strain rate localization zone is very small, and the material between blades has almost a rigid solid movement, evident in figure 11 where the velocity distribution in the material in a intermediate plane ($\theta = 45°$) is almost $v = \omega r$, as in the blades. On the other hand models–2 have a wider shear strain rate localization zone, although it still could be considered a circular failure surface. It has been verified that models with a plateau in the τ vs. $\dot{\gamma}$ constitutive law have a more definite and narrower localization zone. The differences between Bingham and Carreau models are similar but less important than between models–1 and models–2. Apart from that, Carreau models tend to present a wider shear strain rate localization zone and a less homogeneous distribution of velocities around failure surface than Bingham models.

It should be pointed out that the radius where the maximum shear stress is produced in a intermediate plane ($\theta = 45°$) is almost the same in all the examples (table 3). At the blade planes, the maximum value of shear stress is obviously produced at $r = 1$. Therefore the value adopted in classical formulations that consider the failure surface constant at $r = 1$ seems reasonable. However some authors have reported failure surfaces at $r = 1.05\ R_v$ based on experimental observations (in Arvida clay – sensitive and overconsolidated),[25] and even higher values (but in fibrous peat whose fibers extend the failure zone).[50] That should be dependent on the material involved in the test so the result obtained in this simulation could only apply for soft clays. On the other hand, the shear strain rate is not constant on the failure surface, even if the Bingham–1 model is used, where dimensionless $\dot{\gamma}$ varies from 31.3 at $\theta = 45°$ to 39.4 at $\theta = 0°$. This pattern is more pronounced when a wider shear strain rate localization zone is formed: when the Carreau–2 model is used dimensionless $\dot{\gamma}$ varies from 5.5 to 35.4 at the failure surface. Nevertheless the usual assumption that shear strength is constant on the failure surface is quite correct because usually a wide range of $\dot{\gamma}$ has a narrow range of τ. Models–2 simulations have a maximum difference of 10% in τ at the failure surface (table 3).

Note that in figure 9, constitutive laws are expressed in a dimensionless form, by means of angular velocity ω^*. Thus for different values of ω^*, different responses of shear strength are obtained, unless the type–1 model is used. If material behaviour depends on ω^*, a type–2 model constitutive law should be expected, whereas a behaviour independent of ω^* is typical of type–1 models. That is, independence of s_u from ω indicates that shear stress is constant in the range of shear strain rate applied. Note that this behaviour could change for other strain rate ranges, as in triaxial or viscosimeters tests.

6. APPLICATION TO REAL MATERIALS

Numerical simulation of vane test using constitutive laws estimated for actual materials has also been performed. Two materials have been considered: a slurry waste material called red mud and a soft clay. Both require the definition of a relationship between shear stress and shear strain rate, in order to use the above formulation.

Red mud

This material has been extensively studied by Nguyen and Boger.[51] It is a material produced in the extraction process of aluminium from bauxite. It consists of a mixture of oxides dissolved in a plastic liquid which shows some special characteristics like tixotropy (links between particles broken due to the flow), yield stress and non constant viscosity. A particular red mud formed by a concentration of 37.3% of titanium oxide is simulated. Vane result and viscosimeter experimental values corresponding to that red mud are reported by Nguyen and Boger.[51] Vane tests performed with vane radius equal to 1.3 cm and angular velocity equal to 0.1 cycles/min gave $(s_u)_{vane}$ of 126 Pa. Viscosimeter experimental data and least square aproximation by means of three different constitutive models are presented in figure 13. The models used are Bingham, Casson and Herschel-Bulkley.

Table 4 shows some numerical results of the analyses in order to compare the models employed (with $R^* = 1.3$ cm, $\omega^* = 0.1$ cycles/min and $\tau^* = 133.5$ Pa). Note that again $r = 1.01$ is the radius at which the maximum shear strain rate and shear strength is produced irrespective of the model used. The applied torque values are very different. The reason for that is the range of shear strain rate mobilized during the test: 0 to 40 (dimensionless values) which correspond to $\dot{\gamma} = 0$ to 0.42 s^{-1}. In the zoom of figure 13, the different stress level for this range of $\dot{\gamma}$ is clearly highlighted. That zoom shows that a correct interpolation must be used to perform a correct analysis.

The value of $(s_u)_{vane}$ calculated with Bingham model simulations, 136 Pa, is quite similar to $(s_u)_{vane}$ measured by Nguyen and Boger,[51] 126 Pa. Note that Bingham model has been approximated from experimental viscosimeter data at low shear strain rate, but still 10 times larger than the shear strain rate mobilized in the vane test. In general, extrapolation of experimental values from viscosimeters must be used carefully because the range applied in a vane test is very small when compared to that of a viscosimeter.

Soft clay

Soft clays have been extensively studied also by many researchers, but usually a soil mechanics point of view has been employed to define their behaviour. As a consequence of that, constitutive laws suggested for soft clays are presented usually in terms of a stress - strain relationship instead of a stress - strain rate one, even for clays with a high liquidity index. Most of the studies have been carried out using the conventional triaxial test, which can take from a few minutes to one or two hours. Hence rate effects are expected to be less important than in the vane test, where failure is reached in about one minute. Nevertheless, experimental results obtained in viscosimeters have also been published

(figures 5 and 7), although its shear strain range is different from that used in the vane.

In order to obtain a general form of a shear stress – strain rate relationship, information about duration of triaxial tests and rate effects has been used.[33,52,53] A logarithmic relation between shear stress and time to failure has been proposed by many researchers. Typical curves from Lacasse[52] are presented in figure 14. Using strain rate as main variable, this relationship may be expressed as

$$\tau/\tau_r = a\log(\dot{\gamma}/\dot{\gamma}_r) + b, \tag{23}$$

where τ_r is the failure shear strength at reference time, $\dot{\gamma}_r$ is the failure strain rate at same reference time and a, b are constants. If the test is performed at a constant strain rate, $\dot{\gamma}_r$ can be computed from the ratio shear deformation at failure vs. time to failure. Equation (23) shows the effect of increase in shear strength when the test is faster, which is a known behaviour for soft clays.

From the curves of figure 14, a clay with the following constitutive law has been considered (assuming the reference time equal to 140 min and a 3% of the failure shear deformation at that time):

$$\text{Logarithmic model}: \ \tau/\tau^* = 0.13\ \log(\dot{\gamma}/\omega^*) + 1.39, \tag{24a}$$

where τ^* is a shear strength reference value and ω^* the rotation velocity that has been fixed to 12°/min. Also a Bingham and a Carreau models have been considered interpolating the Logarithmic one in the interval $\dot{\gamma}/\omega^* \in [0.1, 40]$:

$$\text{Bingham model}: \ \tau/\tau^* = 1.46 + 0.0042\ \dot{\gamma}/\omega^*, \tag{24b}$$

$$\text{Carreau model}: \ \mu\omega^*/\tau^* = 100\ \left(1 + 7200(\dot{\gamma}/\omega^*)^2\right)^{-0.48}. \tag{24c}$$

As in previous sections, Bingham and Logarithmic models have been approximated with a initial dimensionless viscosity of 100, to avoid infinite viscosity values. Figure 15 shows the shear strain – strain rate curves corresponding to these models. Note that the Carreau model interpolates so well the Logarithmic model that no difference can be observed over the interesting interval.

The results obtained with these models are represented in figures 16, 17 and 18, and they are compared in table 5. As could be expected, Logarithmic and Carreau results are exactly the same, and the shear strain localizated zone originated using the Logarithmic and Carreau models is slightly wider than the one obtained with the Bingham model. However, the value of the radius at which maximum shear strain rate occurs in an intermediate plane is again 1.01 for all the models. Calculated torques are the same for the three models, so the $(s_u)_{vane}$ associated to the simulations will be also the same. Nevertheless if these laws are extrapolated to other strain rate ranges, the predicted behaviour could be very different, as shown in figure 19.

After comparing experimental results (figures 6 and 7) with figure 19, it must be pointed out that Bingham models must be used with caution. It is very important to choose the correct range of applicability when one desires to approximate the actual behaviour of soft clays by Bingham models. However Carreau and Logarithmic models seem to capture better the changing scale between the results of vane test and viscosimeter ones. Therefore, Carreau and Logarithmic models seem to give continuity from the results of the triaxial undrained tests to that obtained from viscometers.

7. SIZE AND TIME EFFECTS

The dimensionless numbers defined in (19) are very useful to analyze the factors that influence the results of the test. For instance, size effects that have traditionally been considered from an empirical point of view, can be studied in a more objective manner with this approach. A relationship between vane shear strength and shear velocity computed as $v = \omega R_v$ was depicted from experimental results by Perlow and Richards.[35] However, that result was based on just few data, and it was not definite. In fact, other authors[15] have reported completely different results. Based on many laboratory small vane tests and field vane tests on Japanese clays, they did not find any sustantial difference between vane sizes, when the same angular velocity, ω, was used.

In fact, according to (19) the mathematical problem is controlled by $N_2 = \mu\omega^*/\tau^*$, as N_1 is usually very small. Thus the problem does not depend on the vane size, but on the rotation velocity, the yield stress and the viscosity. For a particular soil, ω is the fundamental parameter. That applies for soft materials for which the constitutive laws used are reasonable. And it is confirmed by experimental evidence, as the results presented by Tanaka.[15] An attempt has also been made to use the formulation presented above to reproduce the effect of vane rotation (and therefore the time to failure) on the shear strength provided by the vane.

If different rotation velocities are used in the simulation, a relationship similar to equation (5) is expected to be found. Figure 20 presents the results obtained using two models employed previously (Bingham and Logarithmic). If the computed torque is expressed as

$$(s_u)_{vane}/\tau^* = k_1\omega^{k_2}, \tag{25}$$

the values obtained for Bingham model are

$$(k_1)_{Bin} = 1.358 \quad \text{and} \quad (k_2)_{Bin} = 0.052, \quad \text{with} \quad r^2 = 0.95, \tag{26a}$$

where r^2 is the correlation coefficient, and for Logarithmic model are

$$(k_1)_{Log} = 1.395 \quad \text{and} \quad (k_2)_{Log} = 0.037, \quad \text{with} \quad r^2 = 0.99. \tag{26b}$$

These values are consistent with the experimental ones provided Wiesel[30] and Torstensson[33] indicated in equation (5). In particular, Logarithmic model seems to be specially designed to approximate experimental relationships expressed as equation (25). Therefore, time effects seem to be simulated correctly by means of this model based on fluid mechanics principles. This was expected as those effects were measured on soft clays where viscous phenomena are supposed to be important.

In conventional vane tests, viscous forces dominate inertial ones, and the problem depends on N_2 (equation 19). When a fluid constitutive law is used, the torque increases with time up to a limit value, as in figure 18. It is not possible to reproduce a peak in the torque – time curve in this way, unless inertial forces become important. For usual vane velocities, this is not the case, but some measurements at high velocities have also been reported in the literature.[33] Figure 21 shows the effect of inertial forces on the shape of the torque – time curve, in terms of N_1 dimensionless value, using the Bingham - 1 model from

figure 9. Thus, even for that model, at high rotation velocities, inertial effects produce a peak on that curve. This is consistent with the measurements presented in figure 4,[33] where the peak of the curve torque – rotation (or time) is more pronounced when the test is faster, as inertial forces become more important. For the normal velocity range however, a Bingham model can not produce such a peak, and an explanation in terms of softening of the material could be appropiate.

8. CONCLUSIONS

A simulation of the vane test using an Arbitrary Lagrangian – Eulerian formulation and appropiate for soft clays has been presented. As the dominant failure surface is the vertical one, a 2D analysis has been useful enough to study stress distributions. Also, the use of fluid mechanics principles and fluid mechanics constitutive laws have permitted the characterization of time effects in a natural manner, as velocities instead of displacements are the main variables.

The mathematical problem is governed by two dimensionless numbers. They are related to inertial forces (Newton number) and to viscous forces (Reynolds number). Two tests performed with vanes of different sizes and different rotation velocities, can only be compared by means of these numbers. In most cases, at a typical angular velocity and with usual vane dimensions, the problem becomes quasi-static and independent from inertial forces. Thus in this case, the problem is independent from vane radius and density, and it is controlled by the value of $N_2 = \mu\omega^*/\tau^*$ (μ: viscosity, ω^* : rotation velocity, τ^* : characteristic yield stress). Therefore, rotation velocity should be used as main variable to compare different vanes tested on the same soil, provided that the assumptions considered apply (i.e. when 2D conditions are predominant and soft materials are tested).

For soft clays and usual vane conditions, the simulated torque is always increasing with time. Thus a peak in the curve torque – time should be related to other effects as strain softening of the material tested. However, if rotation velocity is increased, inertial effects become more important, and a peak in that curve is always obtained.

Stress and strain rate distributions on the failure surface depend on the constitutive laws adopted for the material, as stated in previous works. However, the position of the failure surface (where maximum shear stresses are developed) has been found to be always at 1. to 1.01 times the vane radius.

Differences around 10% have been found in the shear stress distribution along the failure surface, depending on the material model. Also, amplitude of the shear band is related to that: Bingham models tend to produce more definite shear bands. On the other hand, a yield stress is clearly obtained when results of the vane test are independent of its rotation velocity. That is, when shear stress is constant irrespective of the shear strain rate reached in the test.

To compare triaxial, vane and viscosimeters results, it is necessary to take into account the different shear strain rate mobilized in each test. The same model will give different strengths in each case. Carreau and Logarithmic models seem to reproduce well that change of scale.

Also, the effect of rotation velocity in shear strength has been simulated using this approach. In fact, shear strength increase associated to rotation velocity increase is directly related to the increment of shear strength due to shear strain

increments. The experimental relation between these variables that has been reported in the literature, has been reproduced by means of this approach. Thus time effects, defined in terms of rotation velocity (or time to failure), have been studied in this manner.

Finally, it can be concluded that the use of a fluid mechanics approach has proved to be appropiate for the interpretation of this test when soft materials are involved.

NOTATION

b_i Mass forces vector

c_j Relative velocity

D Diameter

d_{ij} Strain rate tensor

H Height

k_1, k_2 Parameters of the relationship between shear strength and angular velocity

N_1, N_2 Dimensionless numbers

Ne Newton number

n Parameter of shear stress distribution at the top and bottom surfaces

p Hydrostatic pressure (tension positive)

$\bar{p}$ Dimensionless pressure

R^* Characteristic length

R_v Vane radius

Re Reynolds number

r Distance to vane axis

r^2 Correlation coefficient

S_i Area of each finite element

s_u Undrained shear strength

T, T_h, T_v Total torque, torque from horizontal failure surfaces, and torque from vertical failure surface

t Time

$\bar{t}$ Dimensionless time

$\bar{v}$ Dimensionless velocity

v_i Velocity vector

$\hat{v}_j$ Velocity of the reference system

$\bar{x}$ Dimensionless length

x_i Position vector

$\dot{\gamma}$ Shear strain rate

$\dot{\gamma}_r$ Failure shear strain rate at reference time

μ Dynamic viscosity

ω Angular velocity or rotation velocity

ω^* Characteristic angular velocity

ρ Density

σ_{ij} Cauchy's stress tensor

τ Shear stress

τ^* Characteristic stress

τ_r Failure shear strength at reference time

REFERENCES

1. ASTM, 'Standard Test Method for Field Vane Shear Test in Cohesive Soil', *Annual book of ASTM standards*, Standard D2573-72, Vol. 04.08, 346-348, ASTM, Philadelphia, 1993.

2. A. J. Weltman, J. M. Head, *Site investigation manual*, CIRIA special publication, 25, Property Services Agency, London, 1983.

3. Q. D. Nguyen and D. V. Boger, 'Yield stress measurement for concentrated suspensions', *Journal of Rheology*, **27**, 321-349, (1983).

4. M. Keentok, J. F. Milthorpe and E. O'Donovan, 'On the shearing zone around rotating vanes in plastic liquids: theory and experiment', *Journal of Non-Newtonian Fluid Mechanics*, **17**, 23-35, (1985).

5. I. B. Donald, D. O. Jordan, R. J. Parker and C. T. Toh, 'The vane test – A critical appraisal', *Proc. 9th Int. Conf. Soil Mech. Found. Engrg.*, Tokyo, **1**, 81-88, (1977).

6. B. K. Menzies and C. M. Merrifield, 'Measurements of shear stress distribution on the edges of a shear vane blade', *Géotechnique*, **30**, 314-318, (1980).

7. T. Matsui and N. Abe, 'Shear mechanisms of vane test in soft clays', *Soils and Foundations*, **21**, 4, 69-80, (1981).

8. T. Kimura and K. Saitoh, 'Effect of disturbance due to insertion on vane shear strength of normally consolidated cohesive soils', *Soils and Foundations*, **23**, 2, 113-124, (1983).

9. J. A. De Alencar, D. H. Chan, N. R. Morgenstern, 'Progressive failure in the vane test', *Vane shear strength testing in soils: field and laboratory studies, ASTM STP 1014*, A.F. Richards ed., American Society for Testing and Materials, Philadelphia, 117-128, (1988).

10. D. V. Griffiths and P. A. Lane, 'Finite element analysis of the shear vane test', *Computers and Structures*,**37**, 6, 1105-1116, (1990).

11. L. Bjerrum, 'Problems of Soil Mechanics and Construction on Soft Clays', General Report, *Proc. 8th Int. Conf. Soil Mech. Found. Engrg.*, Moscow, **3**, 111-159, (1973).

12. A. S. Azzouz, M. M. Baligh and C. C. Ladd, 'Corrected field vane strength for enbankment design', *ASCE J. Geot. Engrg.*, **109**, 5, 730-734, (1983).

13. C. C. Ladd and R. Foott, 'New design procedure for stability of soft clays', *ASCE J. Geot. Engrg.*, **100**, 7, 763-786, (1974).

14. W. M. Kirkpatrick and A. J. Khan, 'Interpretation of the vane test', *Proc. 10th Int. Conf. Soil Mech. Found. Engrg.*, Stockholm, **2**, 501-506, (1981).

15. H. Tanaka, 'Vane shear strength of a Japanese marine clay and applicability of Bjerrum's correction factor', *Soils and Foundations*, **34**, 3, 39-48, (1994).

16. W. M. Kirkpatrick and A. J. Khan, 'The influence of stress relief on the vane strength of clays', *Géotechnique*, **34**, 3, 428 - 432, (1984).

17. P. H. Morris and D. J. Williams, 'A new model of vane shear strength testing in soils', *Géotechnique*, **43**, 3, 489-500, (1993).

18. P. H. Morris and D. J. Williams, 'Effective stress vane shear strength correction factor correlations', *Canadian Geot. J.*, **31**, 335-342, (1994).

19. J. Donéa, P. Fasoli-Stella, S. Giuliani, 'Lagrangian and Eulerian Finite Element Techniques for Transient Fluid Structure Interaction Problems', *Transactions of the 4th Int. Conf. on Structural Mech. in Reactor Techn.*, paper B1/2, San Francisco, (1977).

20. A. Huerta and W. K. Liu, 'Viscous Flow with Large Free Surface Motion', *Comp. Meth. App. Mech. Engrg.*, **69**, 277-324, (1988).

21. P. Van der Berg, J. A. M. Teunissen, J. Huetink, 'Cone penetration in layered media, an ALE finite element formulation', *Computer Methods and Advances in Geomechanics*, Siriwardane and Zaman eds., 1957-1962, Balkema, Rotterdam, 1994.

22. G. Pijaudier-Cabot, L. Bodé and A. Huerta, 'Arbitrary Lagrangian–Eulerian finite element analysis of strain localization in transient problems', *Int. J. Num. Meth. Engrg.*, **38**, 4171-4191, (1995).

23. A. Rodríguez-Ferran, F. Casadei and A. Huerta, 'ALE Stress Update for Transient and Quasistatic Processes', Accepted to *Int. J. Num. Meth. Engrg.*, (1997).

24. R. J. Chandler, 'The in-situ measurement of the undrained shear strength of clays using the field vane', *Vane shear strength testing in soils: field and laboratory studies, ASTM STP 1014*, A.F. Richards ed., American Society for Testing and Materials, Philadelphia, 117-128, (1988).

25. M. Roy and A. Leblanc, 'Factors affecting the measurements and interpretation of the vane strength in soft sensitive clays', *Vane shear strength testing in soils: field and laboratory studies, ASTM STP 1014*, A.F. Richards ed., American Society for Testing and Materials, Philadelphia, 117-128, (1988).

26. V. Silvestri, M. Aubertin, R. Chapuis, 'A study of undrained shear strength using various vanes', *Geot. Testing J.*, *GTJODJ*, **16**, 2, 228-237, (1993).

27. C. P. Wroth, 'The interpretation of in situ soil tests', *Géotechnique*, **34**, 4, 449-489, (1984).

28. W. J. Eden and K. T. Law, 'Comparison of undrained shear strength results obtained by different tests methods in soft clays', *Canadian Geot. J.*, **17**, 369-381, (1980).

29. G. Aas, 'A study of the effect of vane shape and rate of strain on the measured values of in-situ shear strength of clays', *Proc. 6th Int. Conf. Soil Mech. Found. Engrg.*, Montreal, **1**, 141-145, (1965).

30. C. E. Wiesel, 'Some factors influencing in-situ vane test results', *Proc. 8th Int. Conf. Soil Mech. Found. Engrg.*, Moscow, **1.2**, 475-479, (1973).

31. V. K. Garga and M. A. Khan, 'Evaluation of K_0 and its influence on the field vane strength of overconsolidated soils', *Proc. 13th Int. Conf. Soil Mech. Found. Engrg.*, New Delhi, **1**, 157-162, (1994).

32. P. La Rochelle, M. Roy and F. Tavenas, 'Field measurements of cohesion in Champlain clays', *Proc. 8th Int. Conf. Soil Mech. Found. Engrg.*, Moscow, **1**, 229-236, (1973).

33. B. A. Torstensson, 'Time-dependent effects in the field vane test', *Int. Symp. on Soft Clay*, Bangkok (Thailand), Brenner and Brand eds., Asian Inst. of Technology, 387-397, (1977).

34. V. I. Osipov, S. K. Nikolaeva and V. N. Sokolov, 'Microstructural changes associated with thixotropic phenomena in clay soils', *Géotechnique*, **34**, 2, 293-303, (1984).

35. M. Perlow and A. F. Richards, 'Influence of shear velocity on vane shear strength', *ASCE J. Geot. Engrg.*, **103**, 1, 19-32, (1977).

36. K. T. Law, 'Triaxial-vane tests on a soft marine clay', *Canadian Geot. J.*, **16**, 11-18, (1979).

37. L. Vulliet, K. Hutter, 'Continuum model for natural slopes in slow movement', *Géotechnique*, **38**, 2, 199-217, (1988).

38. D. Rickenmann, 'Hyperconcentrated flow and sediment transport at steep slopes', *J. Hydraulic Engrg.*, **117**, 11, 1419-1439, (1991).

39. J. A. Gili, A. Huerta, J. Corominas, 'Contribution to the study of mass movements: mudflow slides and block fall simulations', *Pierre Beghin Int. Workshop on rapid gravitational mass movements*, Grenoble, CEMAGREF, (1993).

40. T. Berre and L. Bjerrum, 'Shear strength of normally consolidated clays', *Proc. 8th Int. Conf. Soil Mech. Found. Engrg.*, Moscow, **1.1**, 39-49, (1973).

41. F. Komamura and R. J. Huang, 'New rheological model for soil behaviour', *ASCE J. Geot. Engrg.*, **100**, GT7, 807-824, (1974).

42. R. Y. K. Cheng, 'Effect of shearing strain-rate on the undrained strength of clay', *Laboratory shear strength of soil, ASTM STP 740*, R.N. Yong and F.C. Townsend eds., ASTM , 243-245, (1981).

43. G. Mesri, E. Febres-Cordero, D. R. Shields, A. Castro, 'Shear stress – strain – time behaviour of clays', *Géotechnique*, **31**, 4, 537-552, (1981).

44. S. Leroueil, M. Kabbaj, F. Tavenas and R. Bouchard, 'Sress-strain-strain rate relation for the compressibility of sensitive natural clays', *Géotechnique*, **35**, 2, 159-180, (1985).

45. F. Tavenas and S. Leroueil, 'The behaviour of embankments on clay foundations', *Canadian Geot. J.*, **17**, 236-260, (1980).

46. S. P. Bentley, 'Viscometric assessment of remoulded sensitive clays', *Canadian Geot. J.*, **16**, 414-419, (1979).

47. J. K. Torrance, 'Shear resistance of remoulded soils by viscometric and fall-cone methods: a comparison for the Canadian sensitive marine clays', *Canadian Geot. J.*, **24**, 318-322, (1987).

48. J. Locat, D. Demers, 'Viscosity, yield stress, remolded strength, and liquidity index relationships for sensitive clays', *Canadian Geot. J.*, **25**, 799-806, (1988).

49. H. A. Barnes, K. Walters, 'The yield stress myth ?', *Rheologica Acta*, **24**, 323-326, (1985).

50. A. O. Landva, 'Vane testing in peat', *Canadian Geot. J.*, **17**, 1, 1-19, (1980).

51. Q. D. Nguyen and D. V. Boger, 'Thixotropic behaviour of concentrated bauxite residue suspensions', *Reological Acta*, **24**, 427-437, (1985).

52. S. Lacasse, 'Effect of load duration on undrained behaviour of clay and sand - literature survey', *NGI Internal report 40007-1*, Norway, 1979.

53. D. W. Hight, R. J. Jardine A. Gens, 'The behaviour of soft clays', *Enbankments on soft clays*, Special Publication, Bulletin of the Public Works Research Center of Greece, 33-158, (1987).

LIST OF TABLES

FIGURE CAPTIONS

Newtonian	$\mu = \mu_0$	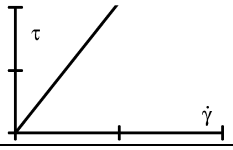
Carreau	$\mu = (\mu_0 - \mu_\infty)\big(1 + (\lambda\dot\gamma)^2\big)^{(n-1)/2} + \mu_\infty$	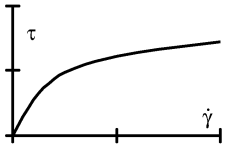
Bingham	$\mu = \infty \quad$ if $\quad \tau \le \tau_0$ $\mu = \mu_p + \tau_0/\dot\gamma \quad$ if $\quad \tau > \tau_0$	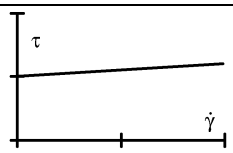
Herschel–Bulkley	$\mu = \infty \quad$ if $\quad \tau \le \tau_0$ $\mu = \mu_p\dot\gamma^{n-1} + \tau_0/\dot\gamma \quad$ if $\quad \tau > \tau_0$	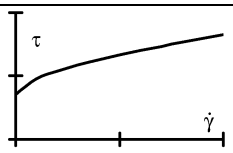
Casson	$\mu = \infty \quad$ if $\quad \tau \le \tau_0$ $\sqrt{\mu} = \sqrt{\mu_p} + \sqrt{\tau_0/\dot\gamma} \quad$ if $\quad \tau > \tau_0$	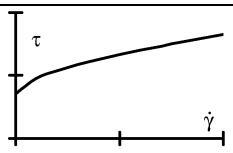

Table 1

	ρ Kg/m^3	R^* m	τ^* Pa	ω^* s^{-1}	N_1	$\min(N_2)$
Red Mud	1200	0.013	126	0.01	1.6E-7	2.E-2
	1200	0.013	126	0.21	7.1E-5	2.E-2
Soft Clay	1400	0.0325	2000	0.0017	2.1E-9	4.E-2
	1400	0.0325	2000	0.0035	9.1E-9	4.E-2
	1400	0.0325	2000	0.0070	3.6E-8	4.E-2

Table 2

	Bin–1	Car–1	Bin–2	Car–2
$\max_{\theta=0^\circ}(v/R^*\omega^*)$	1.00	1.00	1.00	1.00
$\max_{\theta=45^\circ}(v/R^*\omega^*)$	0.95	0.91	0.91	0.78
$r/R^* \mid \max_{\theta=45^\circ}(v/R^*\omega^*)$	0.97	0.97	0.94	0.94
$\max_{\theta=0^\circ}(\dot\gamma/\omega^*)$	39.39	38.74	37.90	35.38
$\max_{\theta=45^\circ}(\dot\gamma/\omega^*)$	31.25	28.04	8.58	5.53
$r/R^* \mid \max_{\theta=45^\circ}(\dot\gamma/\omega^*)$	1.01	1.01	1.01	1.00
$\max_{\theta=0^\circ}(\tau/\tau^*)$	1.00	1.00	1.04	1.02
$\max_{\theta=45^\circ}(\tau/\tau^*)$	1.00	1.00	0.93	0.93
$r/R^* \mid \max_{\theta=45^\circ}(\tau/\tau^*)$	0.95–1.01	1.00–1.01	1.01	1.00
$T/\tau^*(R^*)^2$	6.44	6.44	6.15	6.11

Table 3

	Bingham	Casson	H-B
$\max_{\theta=0^\circ}(v/R^*\omega^*)$	1.00	1.00	1.00
$\max_{\theta=45^\circ}(v/R^*\omega^*)$	0.95	0.92	0.88
$r/R^* \mid \max_{\theta=45^\circ}(v/R^*\omega^*)$	0.97	0.94	0.89
$\max_{\theta=0^\circ}(\dot\gamma/\omega^*)$	39.33	38.67	37.32
$\max_{\theta=45^\circ}(\dot\gamma/\omega^*)$	26.84	11.09	6.63
$r/R^* \mid \max_{\theta=45^\circ}(\dot\gamma/\omega^*)$	1.01	1.01	1.01
$\max_{\theta=0^\circ}(\tau/\tau^*)$	1.01	1.17	0.84
$\max_{\theta=45^\circ}(\tau/\tau^*)$	1.01	1.13	0.75
$r/R^* \mid \max_{\theta=45^\circ}(\tau/\tau^*)$	1.01	1.01	1.01
$T/\tau^*(R^*)^2$	6.51	7.37	4.96

Table 4

	Logarithmic	Carreau	Bingham
$\max_{\theta=0^\circ}(v/R^*\omega^*)$	1.00	1.00	1.00
$\max_{\theta=45^\circ}(v/R^*\omega^*)$	0.88	0.88	0.94
$r/R^* \mid \max_{\theta=45^\circ}(v/R^*\omega^*)$	0.89	0.89	0.94
$\max_{\theta=0^\circ}(\dot{\gamma}/\omega^*)$	38.39	38.34	39.84
$\max_{\theta=45^\circ}(\dot{\gamma}/\omega^*)$	6.70	6.73	10.00
$r/R^* \mid \max_{\theta=45^\circ}(\dot{\gamma}/\omega^*)$	1.01	1.01	1.01
$\max_{\theta=0^\circ}(\tau/\tau^*)$	1.60	1.60	1.63
$\max_{\theta=45^\circ}(\tau/\tau^*)$	1.50	1.50	1.50
$r/R^* \mid \max_{\theta=45^\circ}(\tau/\tau^*)$	1.01	1.01	1.01
$T/\tau^*(R^*)^2$	9.81	9.82	9.85

Table 5

	Logarithmic		Bingham	
ω	$T/\tau^*(R^*)^2$	s_u/τ^*	$T/\tau^*(R^*)^2$	s_u/τ^*
6°/min	9.68	1.51	9.55	1.49
12°/min	9.85	1.54	9.81	1.53
24°/min	10.11	1.58	10.07	1.57
48°/min	10.54	1.65	10.33	1.61
96°/min	11.19	1.75	10.59	1.65

Table 6

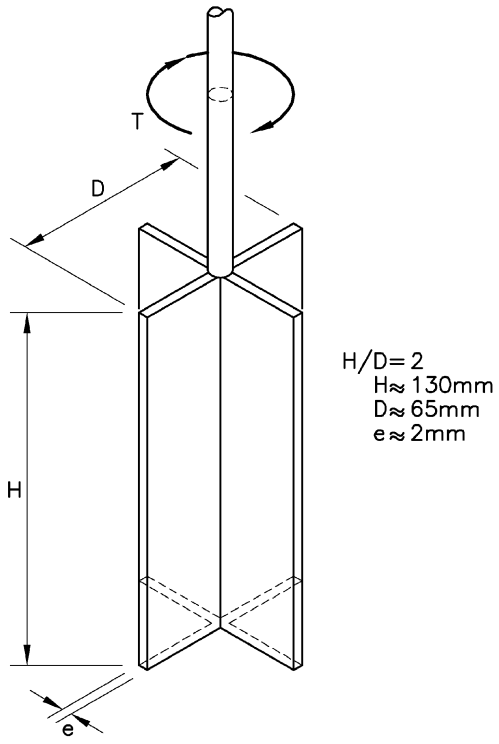

Figure 1

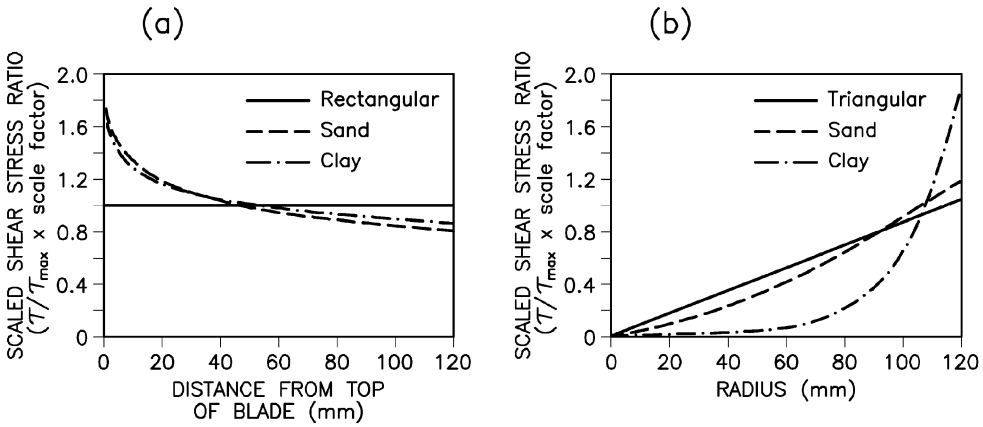

Figure 2

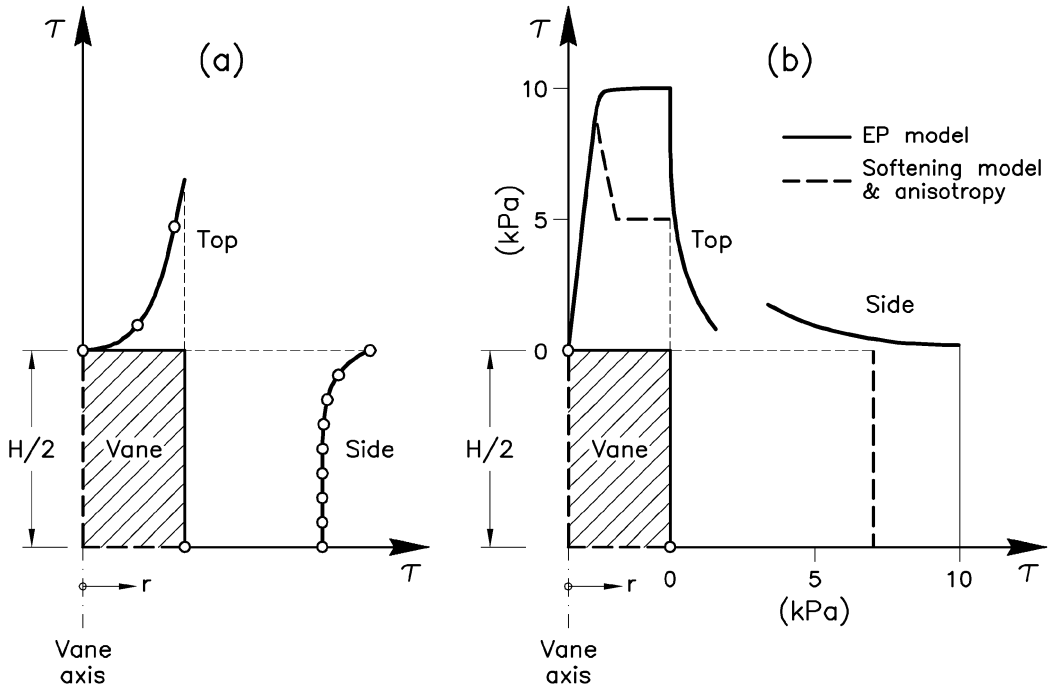

Figure 3

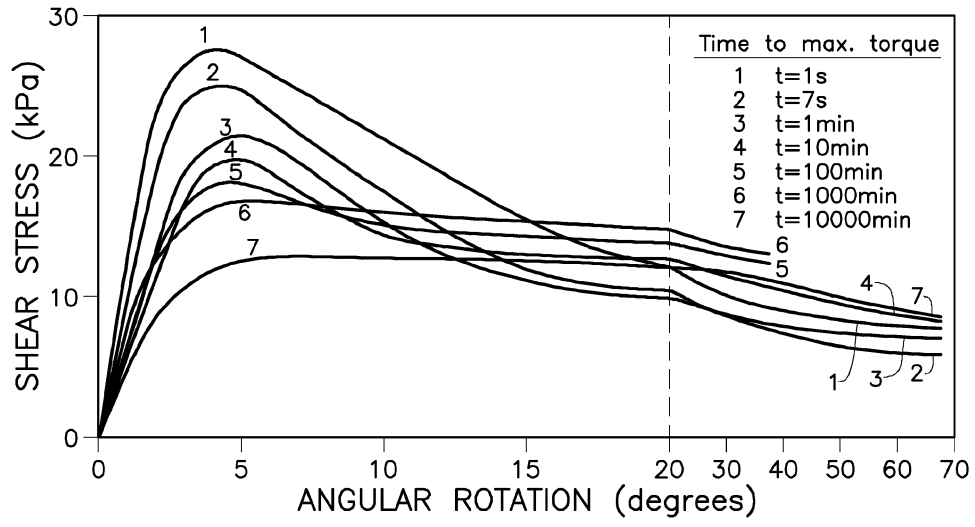

Figure 4

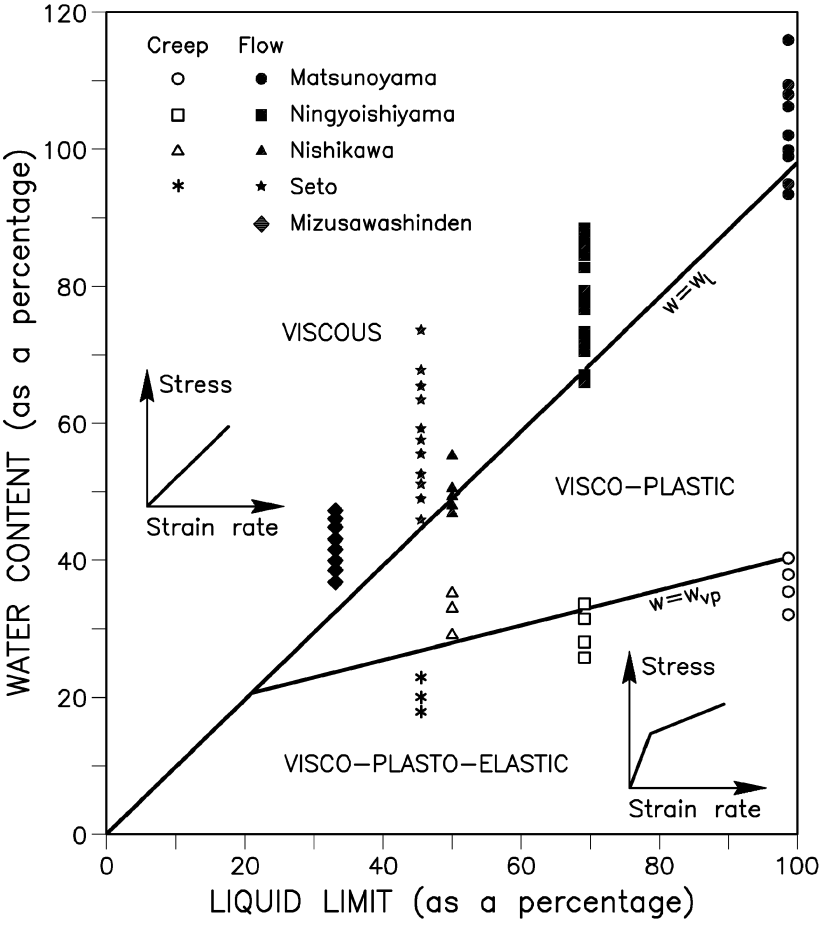
Creep
Flow
Matsunoyama
Ningyoishiyama
Nishikawa
Seto
Mizusawashinden
VISCOUS
Stress
Strain rate
VISCO–PLASTIC
w=wl
w=wvp
Stress
VISCO–PLASTO–ELASTIC
Strain rate
WATER CONTENT (as a percentage)
LIQUID LIMIT (as a percentage)
0
20
40
60
80
100
120

Figure 5

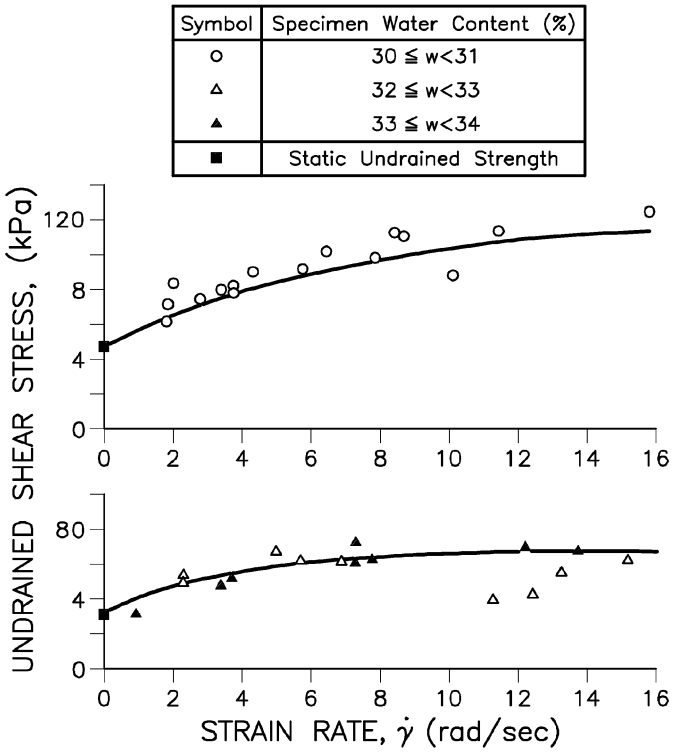
Symbol
Specimen Water Content (%)
30 ≦ w<31
32 ≦ w<33
33 ≦ w<34
Static Undrained Strength
UNDRAINED SHEAR STRESS, (kPa)
120
8
4
0
0
2
4
6
8
10
12
14
16
80
4
0
0
2
4
6
8
10
12
14
16
STRAIN RATE, $\dot{\gamma}$ (rad/sec)

Figure 6

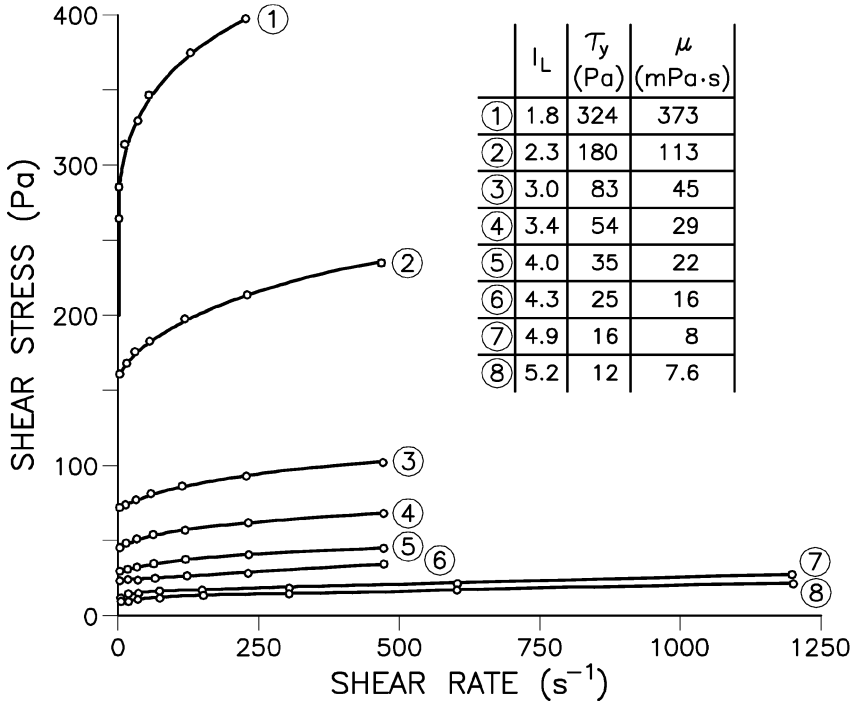

	I_L	τ_y (Pa)	μ (mPa·s)
①	1.8	324	373
②	2.3	180	113
③	3.0	83	45
④	3.4	54	29
⑤	4.0	35	22
⑥	4.3	25	16
⑦	4.9	16	8
⑧	5.2	12	7.6

Figure 7

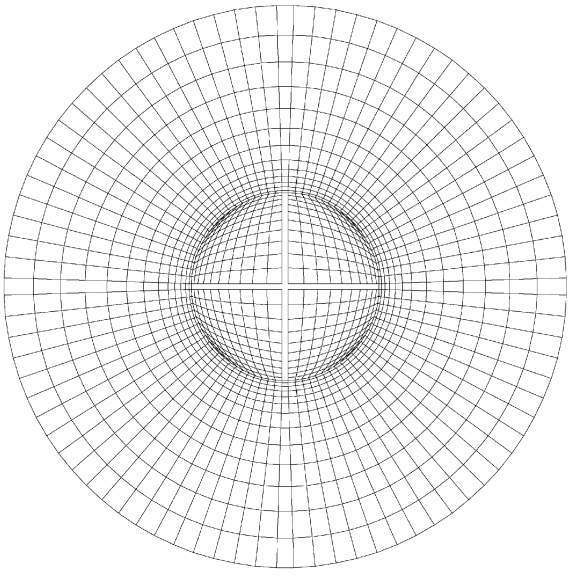

Figure 8

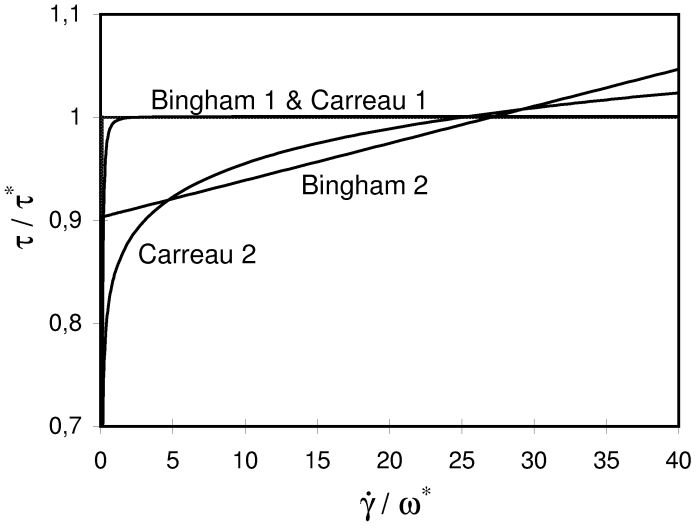

Figure 9

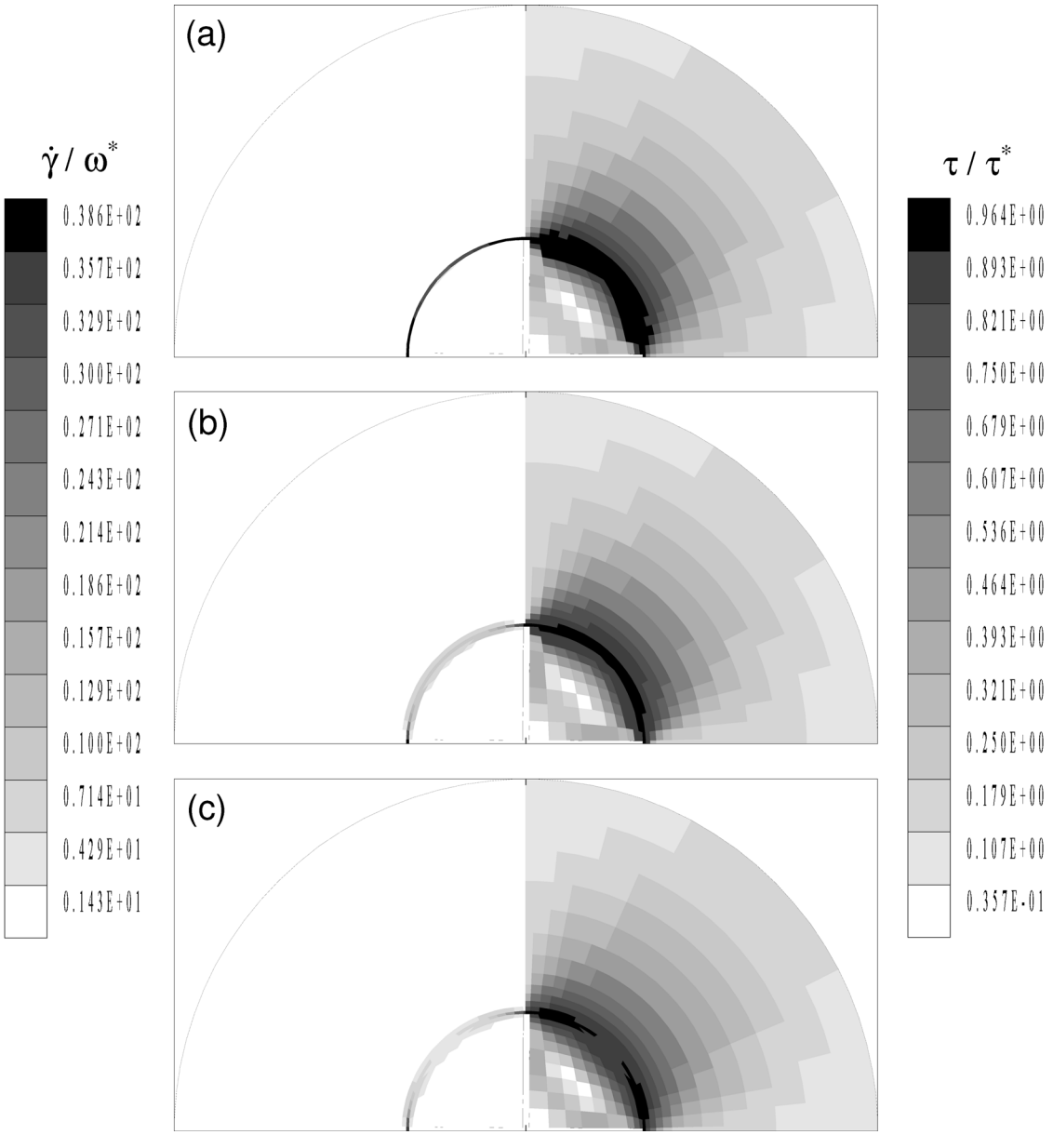
(a)
(b)
(c)
$\dot{\gamma}$ / ω^*
0.386E+02
0.357E+02
0.329E+02
0.300E+02
0.271E+02
0.243E+02
0.214E+02
0.186E+02
0.157E+02
0.129E+02
0.100E+02
0.714E+01
0.429E+01
0.143E+01
τ / τ^*
0.964E+00
0.893E+00
0.821E+00
0.750E+00
0.679E+00
0.607E+00
0.536E+00
0.464E+00
0.393E+00
0.321E+00
0.250E+00
0.179E+00
0.107E+00
0.357E-01

Figure 10

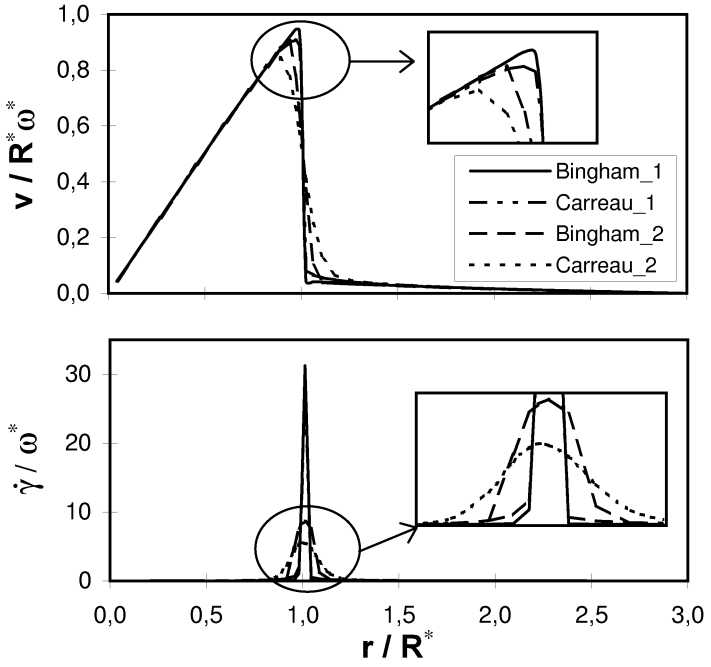

Figure 11

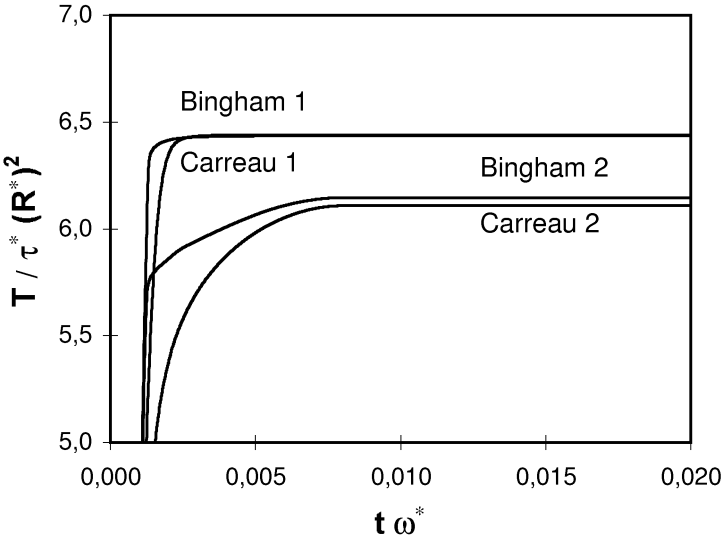

Figure 12

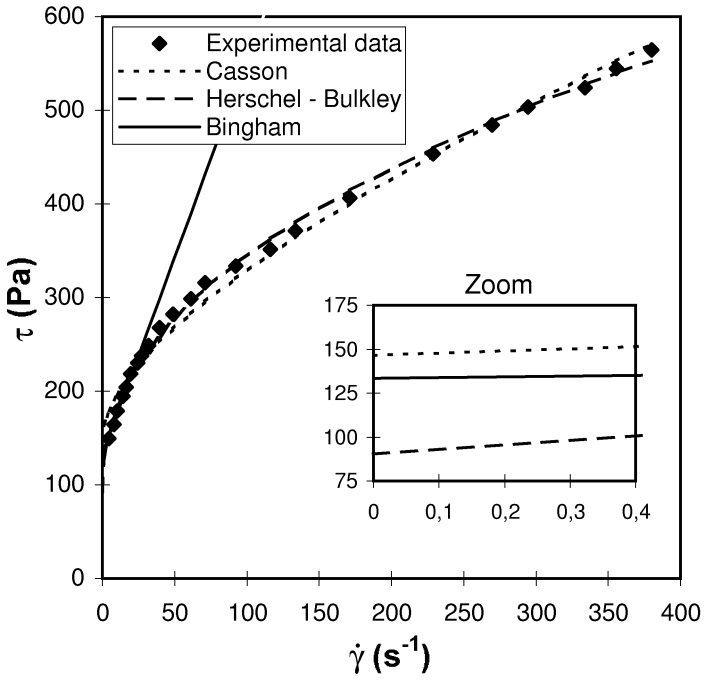

Figure 13

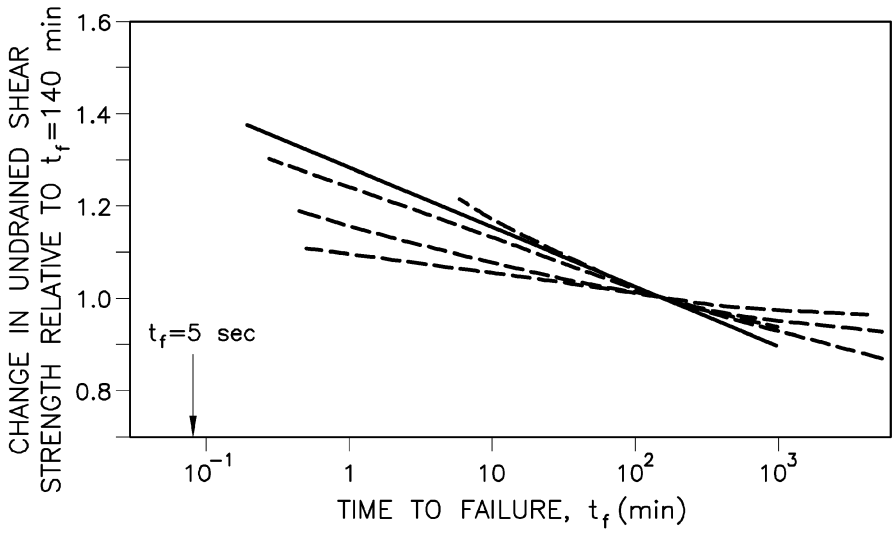

Figure 14

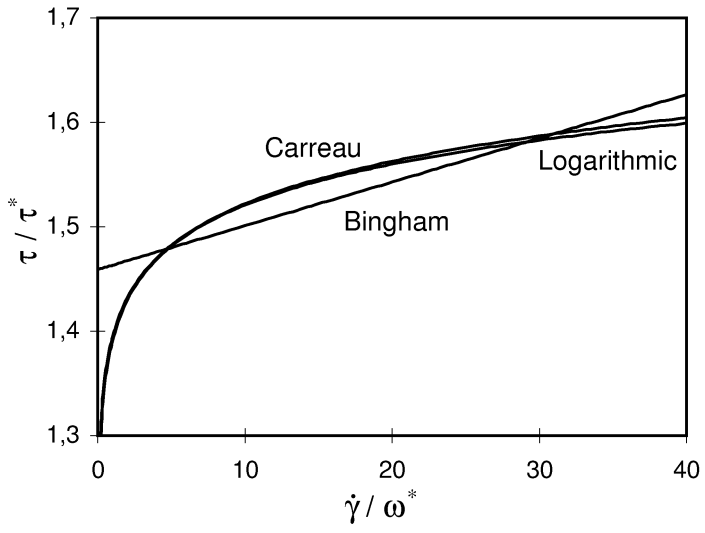

Figure 15

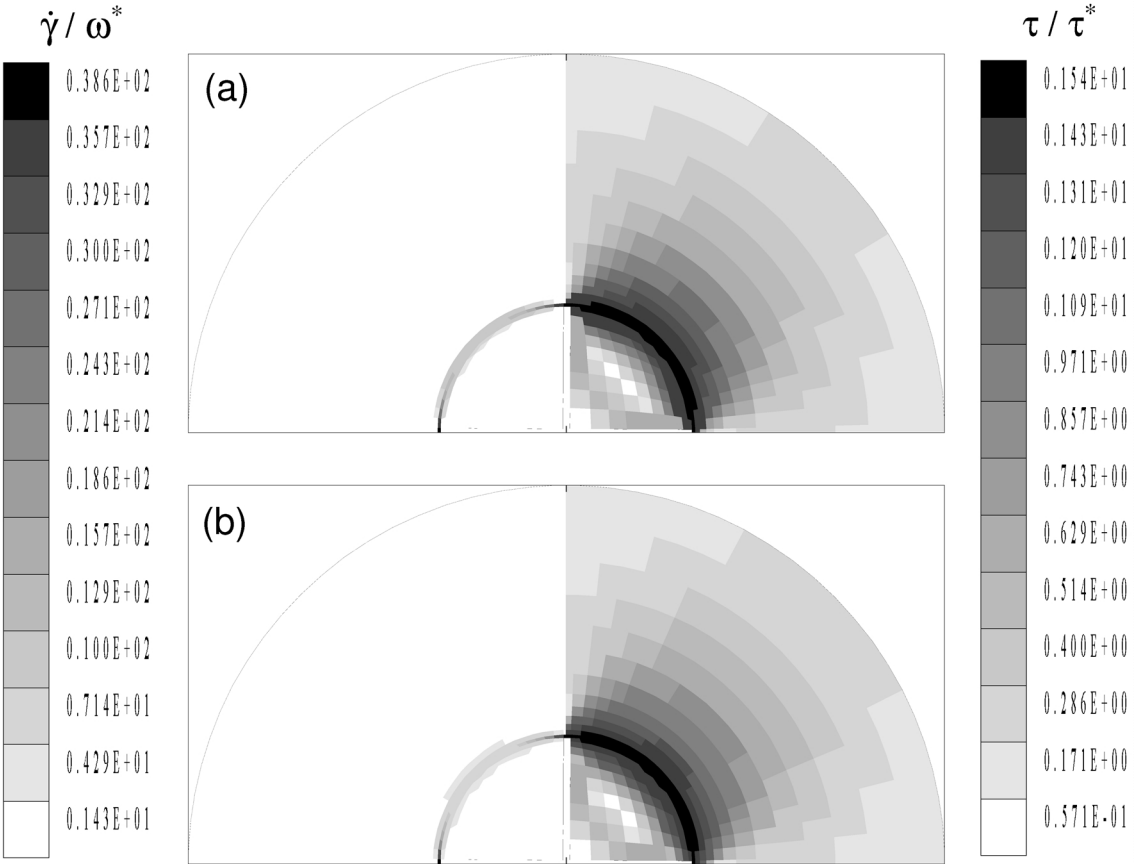
$\dot{\gamma}$ / ω^*
0.386E+02
0.357E+02
0.329E+02
0.300E+02
0.271E+02
0.243E+02
0.214E+02
0.186E+02
0.157E+02
0.129E+02
0.100E+02
0.714E+01
0.429E+01
0.143E+01
(a)
(b)
τ / τ^*
0.154E+01
0.143E+01
0.131E+01
0.120E+01
0.109E+01
0.971E+00
0.857E+00
0.743E+00
0.629E+00
0.514E+00
0.400E+00
0.286E+00
0.171E+00
0.571E-01

Figure 16

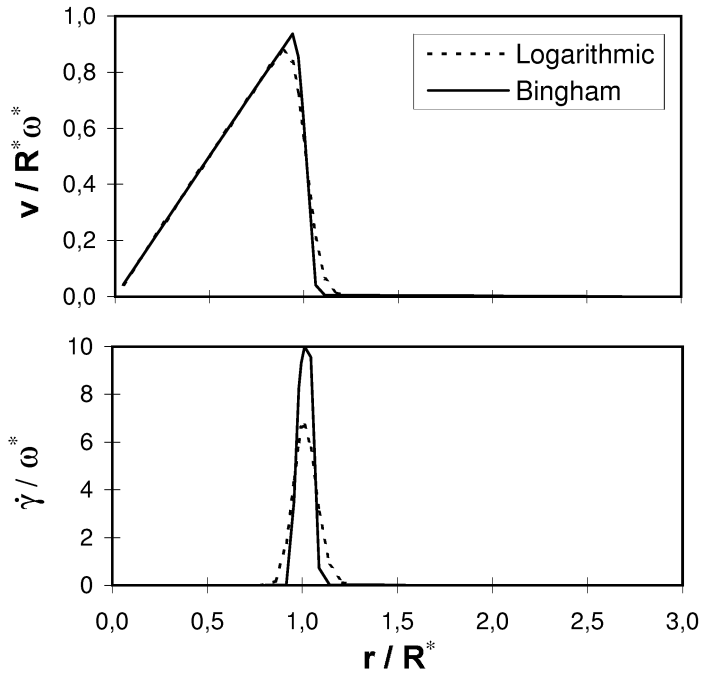

Figure 17

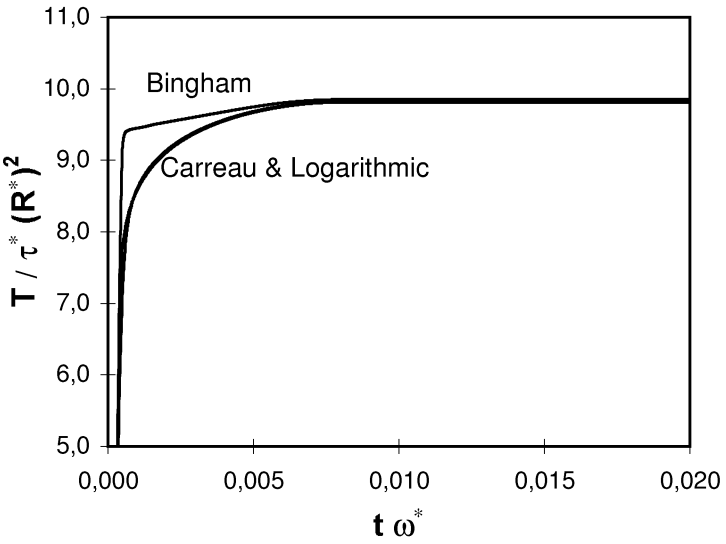

Figure 18

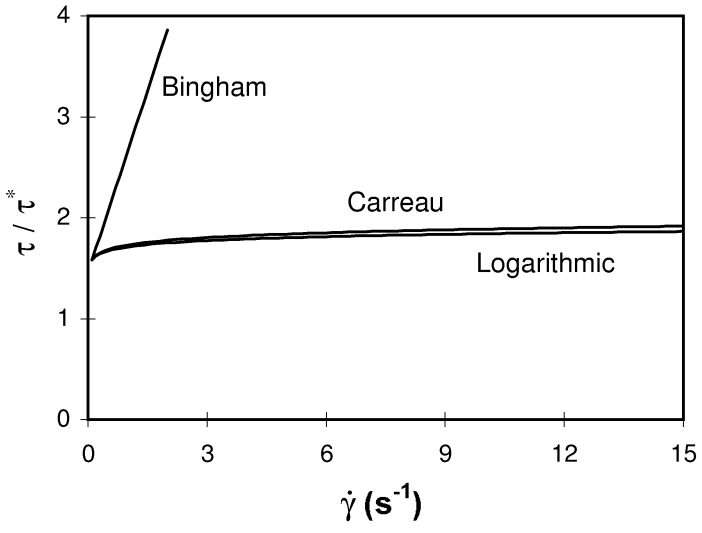

Figure 19

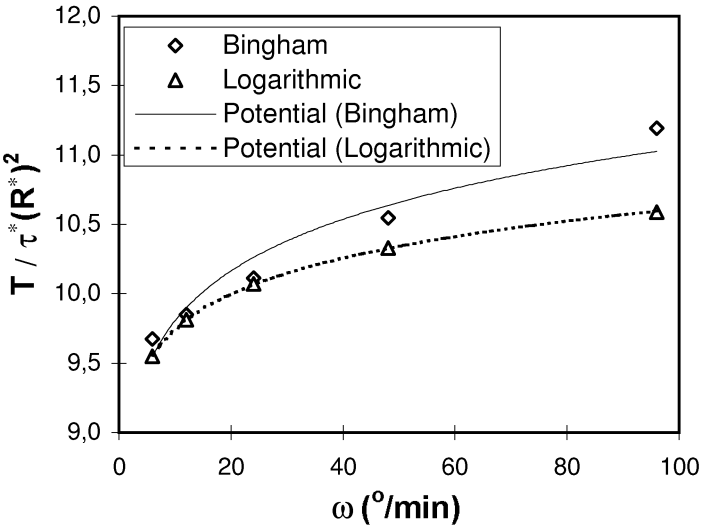

Figure 20

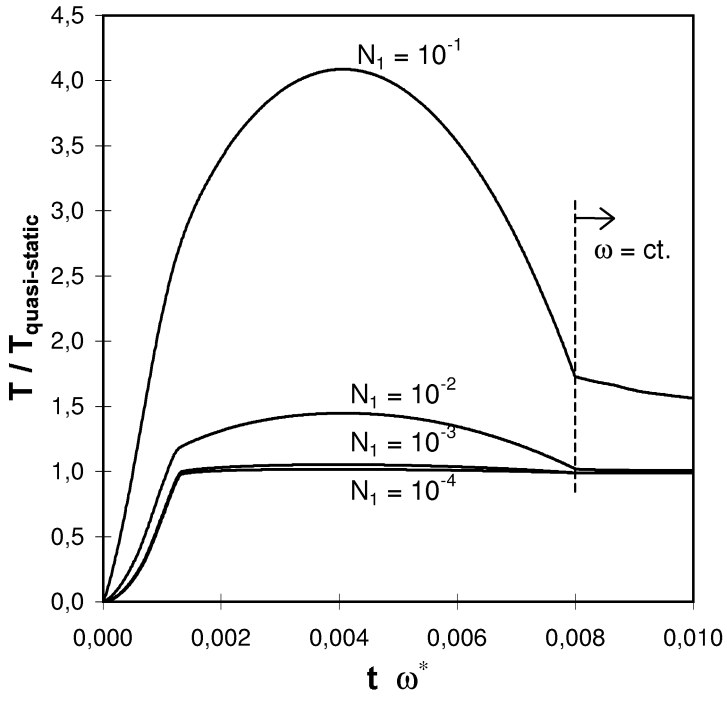
4,5
4,0
3,5
3,0
2,5
2,0
1,5
1,0
0,5
0,0
T / T quasi-static
N1 = 10-1
ω = ct.
N1 = 10-2
N1 = 10-3
N1 = 10-4
0,000
0,002
0,004
0,006
0,008
0,010
t ω*

Figure 21